

# MECHANICAL PROPERTIES OF LASER BEAM WELDED AW2099 ALLOY JOINTS

Milan Marônek<sup>1</sup>, Jozef Bárta<sup>1</sup>, Michaela Lopatková<sup>1</sup>, Katarína Bártová<sup>1</sup>, Matej Pašák<sup>1</sup>,  
Miroslav Sahul<sup>1</sup>, Ján Urminský<sup>1</sup>

<sup>1</sup>*Slovak University of Technology, Faculty of Materials and Technology*

*Keywords: AW2099, welded joint, mechanical properties*

Abstract:

The paper deals with the analysis of mechanical properties of welding joints made of AW 2099 aluminium-lithium alloy by laser beam welding. Static tensile test, microhardness measurement and metallographic analysis were carried out. The results revealed a significant decrease in hardness in the weld joints in the weld metal region, which was also reflected in a decrease of yield strength and ultimate tensile strength. The drop of mechanical properties was caused by the dissolution of precipitates in the weld metal and HAZ. The mechanical properties of the welded joints can be improved by heat treatment consisting of solution annealing and artificial aging.

## 1 INTRODUCTION

Aluminium alloys of 2XXX series are high-strength aerospace alloys in sheet or plate form. Their chemistry makes most of them unweldable using GTAW or GMAW because of hot cracking. The exceptions are 2219 and 2519, which are either readily welded using 2319 or 4043 filler metal. It is very common and very high in strength, but it is extremely crack-sensitive [1].

Hot cracking susceptibility for different aluminium alloys dependant on the Si and Mg content is illustrated in Figure 1. Different solutions to decrease the formation of hot cracking have been reported, for example addition of filler material with increased Si content or the use of dual beam lasers in order to achieve a lower cooling rate [2, 3, 4].

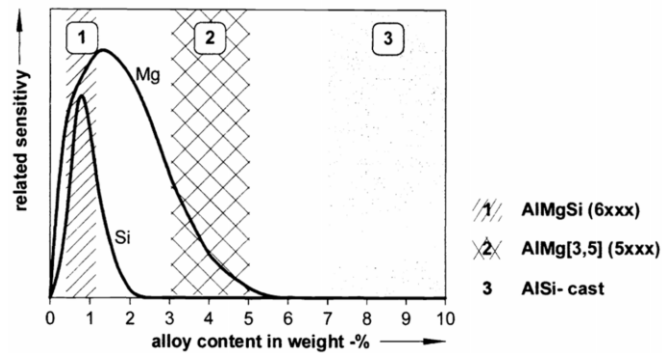


Figure 1. Hot cracking sensitivity of aluminium alloys dependant on Si and Mg content

AW2099 is a high-strength aluminium lithium alloy ideal for use in environments requiring low density, high stiffness, superior damage tolerance and excellent corrosion resistance. The alloy was developed mainly for use in motorsport, aerospace and high strength applications, e.g. production of lower wing stringers, aircraft fuselages and others. Lithium additions increase the strength and modulus of Al alloys while lowering their density. This material grade offers high strength and excellent corrosion resistance with moderate fracture toughness [5].

Pores formed during welding of aluminium are well-known problem. However, the reasons for the formation of pores are not fully understood. Two main reasons for the formation of pores can be found in literature. One explanation is the addition of hydrogen from the aluminium oxide layer from the surface. The pores are then formed due to the low solubility of hydrogen in aluminium during the solidification. Other reports state that the porosity is mainly affected by the stability of the keyhole. Possible solutions to decrease the number of pores in welding of aluminium are addition of filler material with proper Si content, optimised laser power and focal position [2, 6, 7, 8].

Some authors refer that weld porosity can be detrimental to the static tensile properties and bend ductility of weld joints. Tensile elongation drops immediately as the porosity level is increased; whereas, tensile strength is tolerant of some porosity. In their case yield strength was only slightly reduced by porosity levels up to about 4 volume percent. However, it was possible to have acceptable tensile strength and not pass the bend test and radiographic requirements. Volume percent porosity varied exponentially with shield gas dew point. Acceptable welds were made with argon gas having a dew point of +7 F [9].

Since the surface oxide layer causing issues during welding, it has to be removed before the welding. Time between the cleaning and welding needs to be short since the surface layer is relatively quickly formed again. Different solvents are available at the market as well as some mild or strong alkalines. Wire brush need to be used in case of big thickness of oxide layer. For manipulation with parts during the joint assembly the gloves should be used to avoid moisture and grease getting to edges prepared for welding. Shielding gases like argon and helium are mostly used for welding. To

acquire best condition for welding, both surface and root section of weld joint needs to be covered by shielding gas during the welding process. Our previous work was focused on obtaining crackles weld joints with low porosity. The aim of this study was to analyse the mechanical properties of weld joints made of AW 2099, produced by laser beam welding.

## 2 MATERIAL AND METHODS

AW2099 alloy was used within the experiment. This alloy belongs to so called third generation of AlLi alloys. Typical chemical composition of AW2099 alloy is provided in Table 1 and its mechanical properties in Table 2 respectively.

*Table 1. Chemical composition of the AW2099 alloy (Smithmetal 2018)*

Chemical composition [wt. %]												
	Cu	Li	Zn	Mg	Mn	Zr	Ti	Fe	Si	Be	Others	Al
<b>Min</b>	2,40	1,60	0,40	0,10	0,10	0,05					0,05	Balance
<b>Max</b>	3,00	2,00	1,00	0,50	0,12	0,10	0,10	0,07	0,05	0,0001	0,15	Balance

*Table 2. Mechanical properties of the AW2099 alloy (Smithmetal 2018)*

Table 2. AW2099-T8 mechanical properties		
<b>Ultimate tensile strength [MPa]</b>	Parallel to rolling direction	500
<b>Ultimate tensile strength [MPa]</b>	Perpendicular to rolling direction	420
<b>Yield strength [MPa]</b>	Parallel to rolling direction	350
<b>Yield strength [MPa]</b>	Perpendicular to rolling direction	320
<b>Ductility [%]</b>	Parallel to rolling direction	4,5
<b>Young's module [GPa]</b>	-	78

The thickness of the welded samples was 3 mm and was achieved by consequent hot rolling from an initial thickness of 25.4 mm. Solution annealing (530 °C / 1 h) with subsequent quenching to a cold water was applied. The final dimensions of samples to be welded produced by cutting were 100 mm × 70 mm.

Prior to welding, the samples were ground on a surface grinder to remove the oxide layer. The base material (BM) after preparation by grinding had a slight thickness loss about 0.1 – 0.2 mm. The real sheet thickness prepared for welding was 2.8 – 2.9 mm. Right before welding, the weld area was again grinded with a stainless steel brush, and the cutting surface was chemically degreased.

Welding was carried out in CE5AM MTF STU. The laser beam source was a TruDisk 4002 disc laser with a laser head connected to a FANUC M-710ic / 50 robot. The axis of the welds was

perpendicular to the BM rolling direction. Several penetration welds and butt welds were fabricated in the experiment. Based on a visual quality assessment of the surface and root, the welding parameters listed in Table 3 were selected.

Table 3. Welding parameters

Power [W]	Welding speed [mm/s]	Focus [mm]	Argon shielding gas flow rate [l/min]	Helium shielding gas flow rate [l/min]
1700	15	0	30	30

The use of shielding gases as well as the gases distribution played an important role during welding. The example of insufficient shielding gas protection results into weld root irregularities (Figure 2a) as well as weld metal porosity (Figure 2b). The production of sound welds was impossible without special jig and gas protection (Figure 3). The used jig provided continuous protection of the helium atmosphere from the root side. Argon was fed through the gas copper nozzles from the upper side of the weld joint.

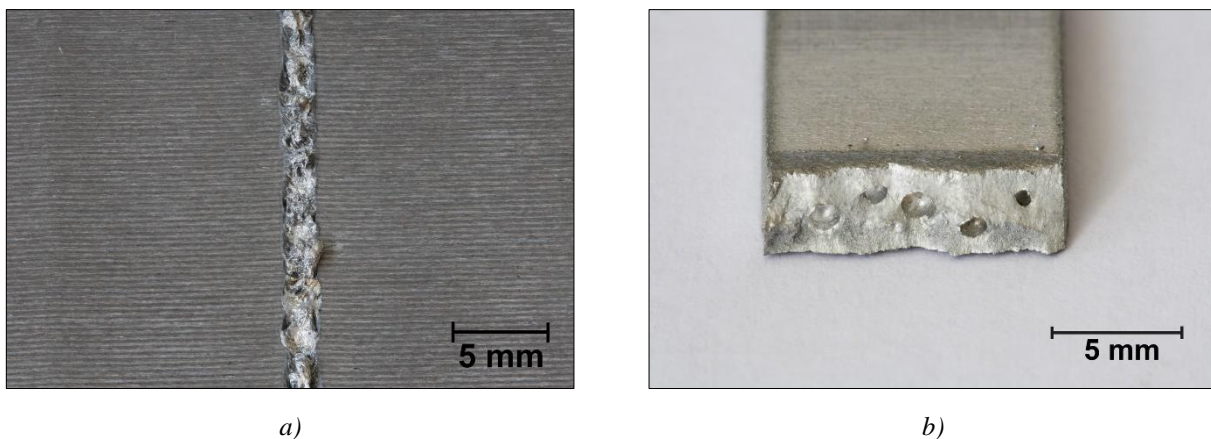


Figure 2. Weld joint defects: a) weld root irregularities; b) porosity in weld metal

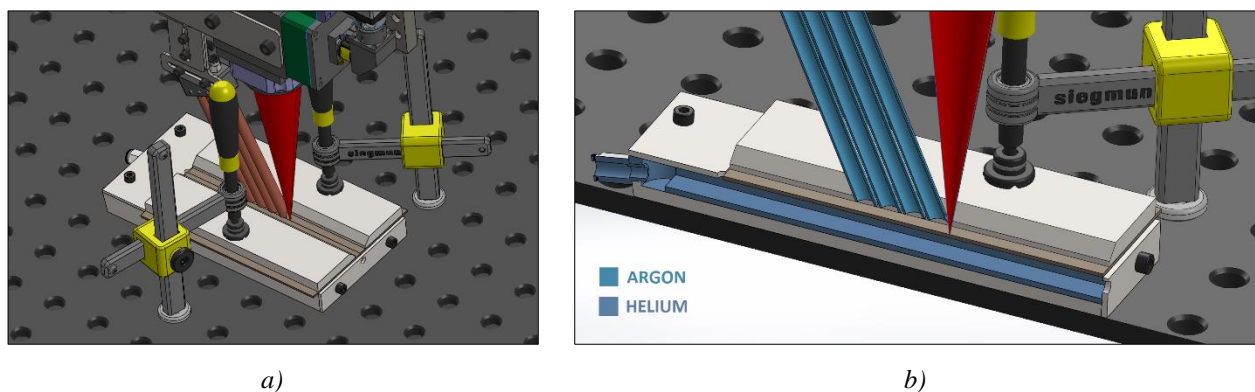


Figure 3. Welding jig: a) experimental setup; b) cross-section of the jig with gas distribution

Weld joint properties and quality were evaluated by the following testing methods:

- visual testing,
- macroscopic analysis,
- microscopic analysis,
- tensile strength test,
- Vickers hardness test.

## 2.1 Mechanical properties testing devices

Welded joint dimensions after welding was  $140 \times 100$  mm. Shape and size of samples for tensile strength test was selected according to the ISO 6892-1 standard (Figure 4). Tensile test samples were cut-off using water jet cutting in order to prevent thermal affection. The placement of tensile test samples on welded joint documents Figure 5.

Tensile strength test was realised in accordance to the EN 10002 standard on LabTest5.250SP1-VM tensile strength testing device. The load was applied in direction parallel to base material rolling process and perpendicular to weld axis.

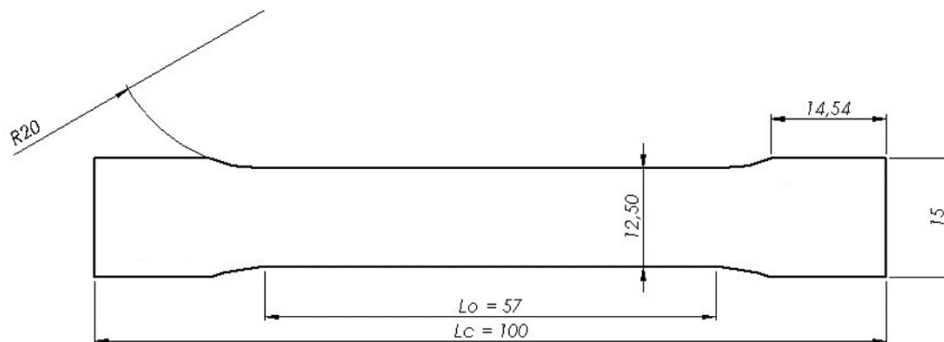


Figure 4. Shape and size of sample for tensile strength test

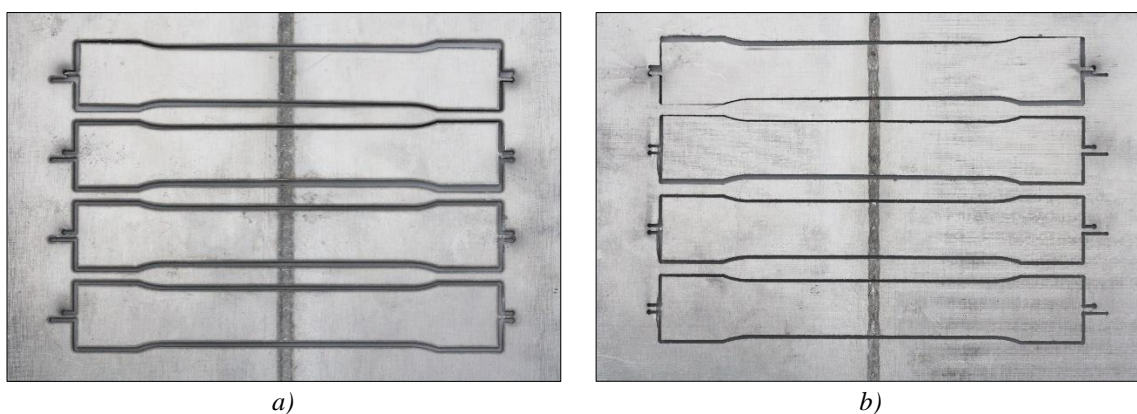


Figure 5. Tensile strength test samples a) surface side; b) root side

The hardness was measured by IndentaMet 1100 hardness tester with a load of 1 N for 10 seconds. The hardness measurement was realised on the cross-section of the sample, in perpendicular direction to the weld axis in two lines.

### 3 RESULTS AND DISCUSSION

The quality of the welded joints was evaluated by visual inspection in accordance to ISO 13919-2. The appearance of the surface and the root of the weld is shown in Figure 6. The quality of the welds was satisfactory despite minor defects such as low spatter on the surface or minor excess root penetration. The excessive porosity was observed during macroscopic analysis and after tensile strength test.

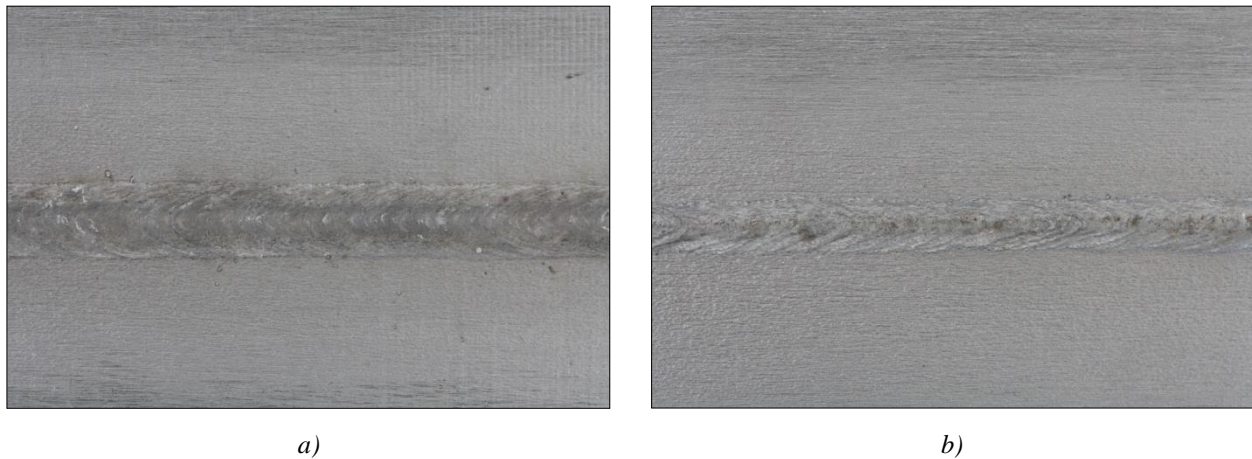
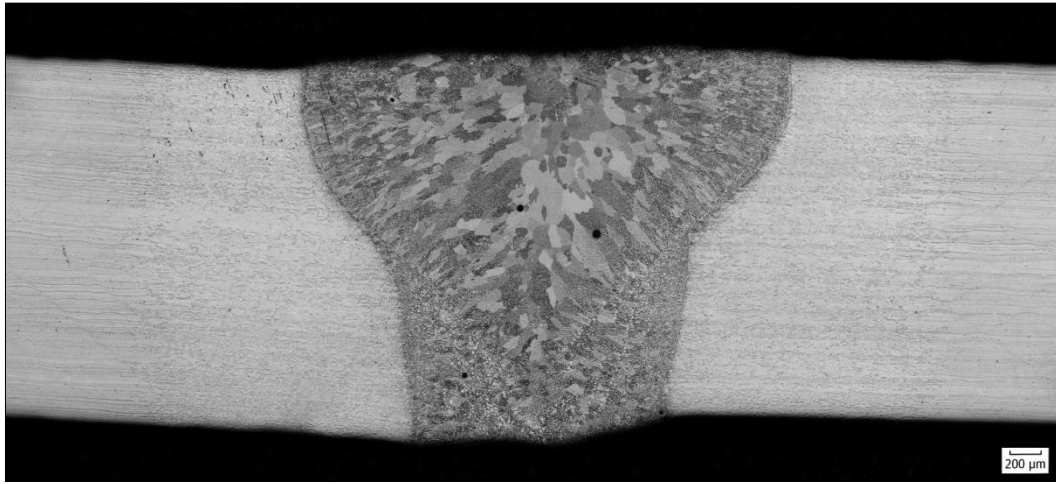


Figure 6. Welded joint appearance: a) surface; b) root

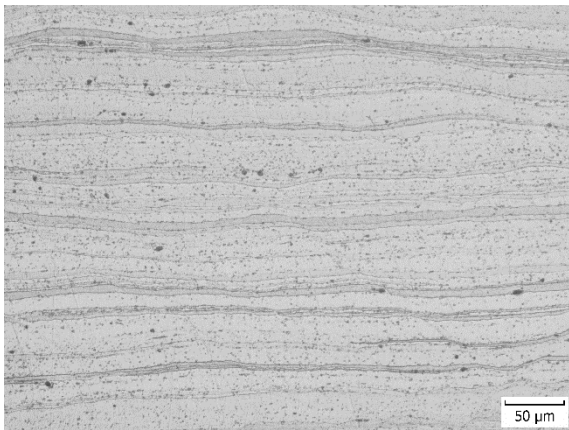
Structural analysis was realised on the cross-section of welded joint. The sample preparation was realised by standard metallography procedure using standard grinding papers and polishing cloths. In order to obtain best surface, the Buehler VibroMet 2 with MasterMet 2 suspension was used as a final step. Keller reagent (95 ml H<sub>2</sub>O, 2.5 ml HNO<sub>3</sub>, 1.5 ml HCl, 1 ml HF) was used in order to reveal the structure. Microscopic analysis was realised using Carl Zeiss Jena Neophot 32 microscope.

The result of macroscopic observation is shown in Figure 7. The weld metal width at the surface was approximately 4 mm and 2 mm at the root side. The heat affected zone was large and reached 1.3 to 2.2 mm. The appearance of the weld was satisfactory, but pores were observed in the weld metal, where the largest one had a diameter of approximately 64  $\mu$ m. The grains had a columnar character towards the axis of the weld, which was related to the heat dissipation during solidification of the weld metal.



*Figure 7. Macroscopy of the weld joint*

Figure 8 a) shows the microstructure of the base material which retained the grain structure after the rolling. Figure 8 b) shows a transition zone from BM to HAZ, with grain recrystallization in the HAZ, which is polyhedral. Figure 8 c) documents the transition from the HAZ to the WM. A fine-grained polygonal structure was observed at the fusion zone. Microstructure of weld metal had dendritic morphology with different grain orientation. The matrix consisted of a solid  $\alpha$  solution (a substitute solid solution of alloying elements in aluminium). A detail of the weld metal is shown in Figure 8 d). Dark areas in the interdendritic spaces may be related to the occurrence of precipitates.



*a)*



*b)*

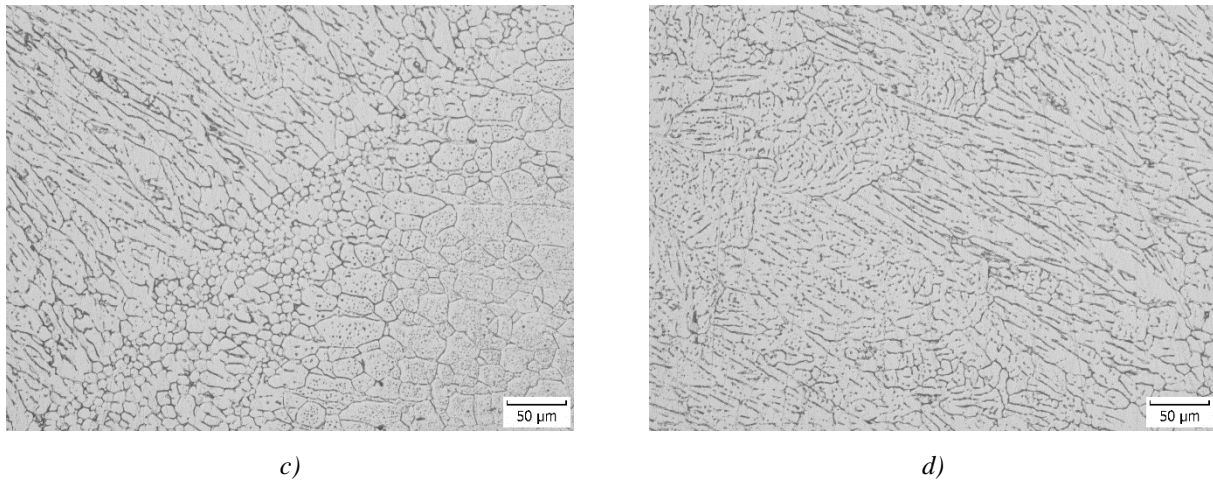


Figure 8. Microstructure of weld metal a) BM; b) BM-HAZ; c) HAZ-WM; d) WM

Figure 9 shows the stress-strain curve of the base material and welded joint samples. Base material had an insignificant yield strength of 423 MPa and ultimate tensile strength of 445 MPa (Figure 9a). Figure 9b documents that the tested sample with a welded joint had a proof yield strength of 265 MPa and an ultimate tensile strength of 273 MPa. The ultimate tensile strength of welded joint was 61.4% in comparison to the base material.

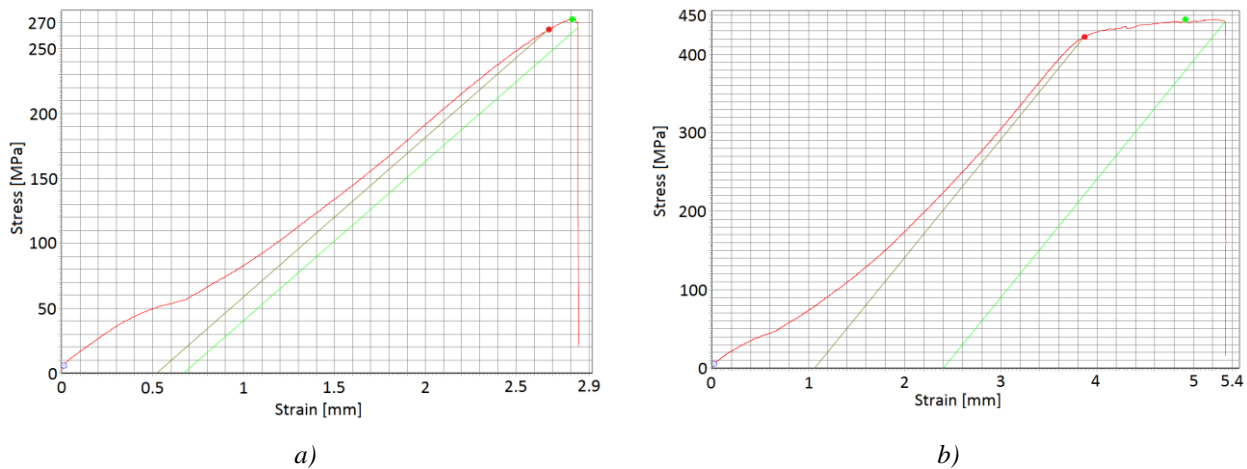


Figure 9. Tensile strength test results a) base material; b) welded joint

The results of the proof yield strength ( $R_{p0.2}$ ), ultimate tensile strength ( $R_m$ ) and elongation ( $A$ ) are given in Table 4. The mean values of the results together with the standard deviation are calculated based on four values from both sample series. While testing welded joints, the crack after the tensile strength test was observed in the area of weld metal.

Table 4. Average values of mechanical properties obtained from static tensile test

Sample	$\overline{R_{p0,2}}$ [MPa]	$\overline{R_m}$ [MPa]	$\overline{A}$ [%]
BM	422.50±0.71	446.50±2.12	4.32±1.20
WM	272.25±7.18	282.00±15.12	1.48±1.31

Figure 10 documents the hardness profile measured in two lines on welded joint. One line was close to the surface and second one close to the weld root. The average hardness of base material was approximately 111 HV0.1, whereas the weld metal hardness was only 77 HV0.1. The maximum hardness of 120 HV0.1 was measured at fusion zone.

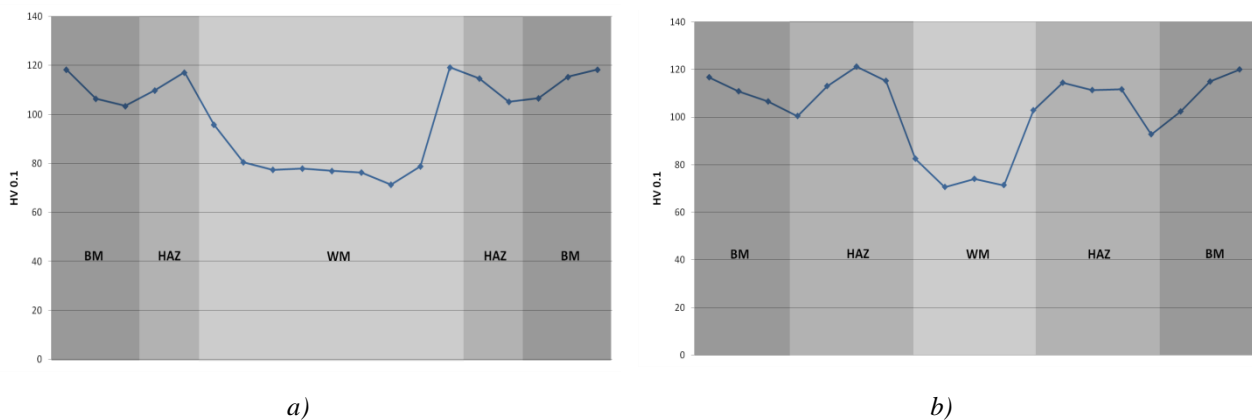


Figure 10. Hardness profiles a) surface line; b) root line

## 4 CONCLUSIONS

Based on realised experiments and evaluation of obtained data it is possible to state the following:

- prior to welding of Al-Li alloys by laser beam, it is very important to clean the surface of welded materials from oxides and grease. Insufficient cleaning results in excessive porosity in the weld metal,
- during welding, it is necessary to protect both the surface and the root of the weld along its entire length,
- helium gave better results in protecting the weld root in comparison to argon,
- the flow rate of shielding gases should be selected at the upper limit of the recommended values. In our case it was 30 l / min,
- the ultimate tensile strength of the welded joints reached only 61% of the ultimate tensile strength of the base material. This drop was caused due to the dissolution of precipitates in the weld metal and HAZ,

- in welded joints, a decrease in hardness in the area of the weld metal of approximately 30% compared to the base material was observed,
- to improve the mechanical properties of welded joints, using heat treatment by dissolving annealing and subsequent artificial aging is highly recommended.

## 5 ACKNOWLEDGEMENT

This work was supported by the Slovak Research and Development Agency under the contract No. APVV-15-0337.

## 6 REFERENCES

- [1] Frank Armao, Weldable and unweldable aluminum alloys, Accessed 5.9.2019, Available online <<https://www.thefabricator.com/article/aluminumwelding/weldable-and-unweldable-aluminum-alloys>>
- [2] D. Löveborn, J.K. Larsson, K.-A. Persson, Weldability of Aluminium Alloys for Automotive Applications, Physics Procedia, Volume 89, 2017, Pages 89-99, ISSN 1875-3892, <https://doi.org/10.1016/j.phpro.2017.08.011>.
- [3] M. Kutsuna, S. Kitamura, K. Shibata, H. Sakamoto, K. Tsushima Improvement of the joint performance in laser welding of aluminium alloys, Welding in the World, 50 (2006), pp. 22-27
- [4] J. Xie Dual Beam Laser Welding, Welding Journal, 81 (2002), pp. 223-230
- [5] SHP 2099 Ultimate Datasheet, SMITH High Performance, Accessed 5.9.2019, Available online <<https://www.smithshp.com/shp-2099-ultimate.htm>>
- [6] L.A. Pinto, L. Quintino, R.M. Miranda, P. Carr Laser Welding of Dissimilar Aluminium Alloys with Filler Materials, Welding in the World, 54 (2010), pp. 333-341
- [7] Pastor, M., Zhao, H., Martukanitz, R.P., Debroy, T., 1999. Porosity, Underfill and Magnesium Loss during Continuous Wave Nd: YAG Laser Welding of Thin Plates of Aluminum Alloys 5182 and 5754. Welding research supplement, 207-219.
- [8] Fahlström, K., Janiak, P., 2012. Aluminium joining for automotive applications. Swerea KIMAB AB.
- [9] Rudy J F and Rupert E J: 'Effects of porosity on mechanical properties of aluminium welds' Welding Journal, July 1970, pp322-s-337-s.